DFG 1/2

Crack Arrest Based Safety Analysis for a Reactor Pressure Vessel Under Emergency Cooling Conditions

J.G. Blauel

Fraunhofer-Institut für Werkstoffmechanik, Wöhlerstr. 11, D-7800 Freiburg, Germany

G. Nagel

Nordwestdeutsche Kraftwerke AG, Abt. Kraftwerk, Pappelallee 35-37, D-2000 Hamburg 76, Germany

Abstract

The tools of linear-elastic fracture mechanics were used to quantify the margin of safety against brittle failure of a reactor pressure vessel under conditions of a LOCA. For this purpose in a wide parameter study it was investigated whether hypothetical cracks in the core region could initiate for possible material conditions between begin and twofold end of life and if yes, at which final crack depth they would arrest. In the analysis a finite crack geometry, the cladding, a radial variation of the neutron fluence in the wall and their influence on the material toughness in the critical belt line weld as well as a possible warm prestress effect have been taken into account.

1. Introduction

In connection with a number of alterations of the reactor protection system including hot leg high pressure injection the safety analysis for the pressure vessel of KKS - that is a 600 MW PWR at Stade operating since 1972 - had to be updated (BLAUEL /1/; NAGEL /2/; KAUN, KÖHRING /3/). Especially, new loading transients, realistic crack sizes, and an improved material data base should be taken into account. Using the tools of fracture mechanics together with complete finite element analyses conditions for exclusion of crack initiation and the potential to arrest initiated cracks should be quantified.

The results presented have been generated in an joint effort by a number of colleagues at IWM and NWK; their contributions are gratefully acknowledged.

2. Stress analysis

Figure 1 gives an overview of the three major steps of the fracture mechanics analysis. Figure 2 summarizes the main geometrical and the loading conditions used in the analysis. The core region of the pressure vessel can be described as a long open cylinder with a inner radius R = 2047 mm and a wall thickness of W = 192 mm including 7 mm of austenitic cladding on the ferritic (22 Ni Mo Cr 37 = A 508 CL 2) base material. A near-core circumferential weld extends over 40 to 80 mm height.

If during emergency core cooling (ECC) conservatively cooling of the whole inner surface is assumed a temperature field develops which is only a function of the radial coordinate. The induced thermal stresses in axial direction are highest with tension at the inner surface and their influence on hypothetical circumferential cracks (plane and simple contoured, infinite or of finite length) have been analysed.

After changing to hot leg injection spring 1985 no longer small primary circuit leaks with high remaining pressure produce the most severe situations for the vessel. A thermohydraulic analyses of the utility and the TÜV have shown an ideal thermal shock

$$T = 288 \quad 20^{o}C \text{ at } p = 2 \text{ MPa}$$

to be the most critical transient enveloping all upset and emergency conditions.

The temperatures in the vessel wall resulting from this transient have been calculated using a finite difference code taking into account a smoothing effect of the cladding by a modified heat transfer coefficient.

The temperature gradients together with the constant internal pressure and an assumed cosine distribution of residual stresses give rise to axial stresses σ_z as a function of distance into the wall and time into transient which are calculated using the finite element code ADINA. Available closed form solutions give slightly conservative results as compared to FEM.

The weight functions approach of LABBENS et al. /4/ has been used to evaluate stress intensity factors for complete circumferential cracks. The results have been found very accurate for crack depth upto 0,7W 150 mm through a comparison with finite element analyses. A small scale plastic zone correction according to ASME XI is used in all cases to determine an effective crack depth. But the correction is small for relevant times in the transient as has been shown by an elastic-plastic FE-analysis. In Fig. 3 the resulting K for the combined loading by internal pressure, thermal shock and residual stresses are plotted against the respective crack front temperature which varies with time. The curves have to be read from right to left i.e. from the high service temperature of 288^{o}C to the low temperature of the cooling medium. Relative maxima are reached for all crack depths within the first 7 to 10 minutes. The maxima increase with crack depth a and are shifted to later times at higher temperatures. At about a = 100 mm an absolute maximum of K_I = 200 MPa m is surpassed.

Long axial cracks produce higher K-factors as compared to complete circumferential cracks under the same loading. But the irradiation surveillance programs have shown that only the weld material properties are impaired by the neutron embrittlement. The HAZ and base material toughness remains unchanged. Then it could be shown by a separate fracture mechanics analysis (PETERS and BLAUEL /5/) that assumed axial cracks cannot grow longer than the width of the embrittled weld material and cannot grow deeper than 1/4 of the wall thickness with resulting K-factors smaller than the corresponding circumferential cracks.

For finite length circumferential cracks stress intensity factors have been evaluated for the apex and the surface points using analytical approximations. A comparison with 3D FE calculations as in Fig. 4 shows these formulas to deliver conservative results. For a crack with an aspect ratio of 1:3 the SIF's are about 30 % smaller than for the corresponding infinite crack.

The cladding has some stiffening effect on the vessel regime close to the crack and causes a reduction of the stress intensity under thermal shock loading. The investigations of

ERDOGAN /6/, which are summarized in Fig. 5, have shown a reduction of about 30 % for shallow underclad-cracks as compared to results of Fig. 3 neglecting the cladding as a load bearing part.

3. Material characterization

Through intensive testing of irradiation surveillance specimens of the high copper Stade weld material and of material from a reference weld irradiated in a research reactor a rather complete picture of the fracture mechanics material properties is available. Figure 6 summarizes the results for the initiation fracture toughness K_{IC} as a function of integrated neutron fluence and of temperature (NAGEL /2/). The curves are derived from a regression analysis of ASTM-valid test results from WOL specimens (upto 100 mm thick) and they form lower bounds to the critical KKS weld material. With increasing fluence the curves are shifted to higher temperatures and their slopes change.

After the 8th operating cycle the fuel loading of the core has been modified by inserting expired fuel elements and absorber rods in external positions of the principal axes. By these measures the strong azimutal variation of the fluence is smoothened and the end of life value will be limited to about 1.7 10^{19} n/cm^2 for E 1 Me V. Self attenuation of the fluence and therefore an increase of toughness properties through the vessel wall is taken into account in the analysis to follow.

Crack arrest toughness values K_{Ia} for the embrittled weld material have been derived using the ASME XI recommendation, i.e. a 43°C temperature shift against the relevant K_{Ic}-curve (Fig. 7). The conservatisme of this procedure has been checked using the latest data of an ASTM cooperative test program on crack arrest (BEINERT and KALTHOFF in /1/).

4. Safety assessment

The safety assessment relies on a comparison of the local loading conditions at the crack front

$$K^{ges} = K_I\ (a, 2c, t, p_i, T, \sigma_e)$$

and the material resistance against crack initiation

$K_{Ic} = K_{Ic}$ (T, o) as well as for crack arrest $K_{Ia} = K_{Ia}$ (T,o).

This is realised by aid of the IWM-computer program "Thermo arrest" in so called "critical crack depth vs time"-diagrams as first introduced at ORNL (BALL et al. /7/). Figure 8 describes the situation in the vessel for an inner surface fluence of 0,9 10^{19} n/cm^2 which will be reached in 1986: There is obviously no depth a of hypothetical circumferential cracks which is initiated at any time in the critical transient considered.

The same situation is again shown in Fig. 9: For no crack depth a at no time in the transient the loading K_I at the crack tip becomes greater than the material toughness K_{Ic} for the relevant conditions of fluence (incl. self attenuation) and temperature. The load path of the 14 mm deep crack is closest to the relevant material K_{Ic}-curve with a distance of at least 2 K. For the safely detectable crack depth of 2 mm (see /3/) the distance is 31 K corresponding to an additional lifetime of more than 10 years.

Figure 10 describes the anticipated EOL-situation with a surface fluence of 1.7. 10^{19} n/cm^2. All cracks smaller than a/W = 0,021 that is a = 4 mm cannot initiate; never in the transient for these cracks K_I K_{Ic}. Deeper cracks, i.e. cracks with 4 a_i 50 mm will initiate and will extend until K_I gets smaller than K_{Ia} and they are arrested. They may be reinitiated but the maximum crack arrest depth is 92 mm which is less than 50 % of the wall thickness.

In an extensive experimental program and a theoretical analysis based on work by CHELL et al. /8/ it was shown (HOLLSTEIN and BLAUEL /9/), that credit can be taken of the beneficial effect of warm prestressing (WPS) for the prevailing material and loading conditions of KKS. Therefore, lines of an effective WPS fracture toughness equal to the maximum stress intensity level each crack has experienced before at a higher temperature during the LOCA-transient are drawn in Figs. 8 and 10. They show that crack initiation can be excluded at all for these situations.

The initiation/arrest analyses have been extended to finite length circumferential cracks also. The analysis in Fig. 11 is done stepwise starting from a depth a_o = 10 mm and different lengths c_o. The stress intensity factors are calculated at the apex and at the surface using an averaging procedure according to CRUSE and BESUNER /10/ and they are compared for all times in the transient to the relevant fracture toughness to predict initiation. At the time of first initiation the crack is extended until the loading K_I again becomes smaller than K_{Ia} and the crack is arrested; then locus and time for a further initiation are looked for.

The short cracks grow longer at the very beginning of the transient and they become as long as 2 c   8 W   1.6 m and then they grow into the depth as far as the infinite cracks do. Quantitatively this is a consequence of the high temperature stresses near the inner surface of the vessel and of the low toughness at low temperatures for all fluences in the life of the vessel.

5. Summary and Conclusions

A high safety barrier against vessel failure is demonstrated by the preceeding results. Especially it can be stated for the loading condition defined by the critical transient in Fig. 2 for the time after installation of the hot leg injection system:

- initiation is possible for the first time at a fluence of 1,01 10^{19} n/cm^2 and for crack depths of complete circumferential cracks between 6 and 36 mm with a maximum crack arrest depth of 76 mm which is clearly smaller than a crack depth necessary for plastic collapse of the remaining ligament (Fig. 12)
- but non destructive inspection has shown that no cracks exist in the ferritic weld material deeper than 2 x 2 = 4 mm, therefore crack initiation is not possible at all
- if load path dependent effective K_{Ic}-values are considered (WPS !) first initiation is possible at a fluence of 2,01 10^{19} n/cm^2 for crack depths between 5.9 and 30 mm, which is beyond anticipated EOL-conditions; the maximum arrest crack depth then is 42 mm being againfar away from conditions of possible ligament collapse.

References

/ 1 / BLAUEL, J.G., "Sicherheitsanalyse RDB-KKS 1984", Report IWM V 30/84, August 1984

/ 2 / NAGEL, G., "Zweiter Statusbericht zur Sicherheitsanalyse des KKS-RDB. Aktualisierte Fassung mit Stand Oktober 1984". Report NWK, Oktober 1984

/ 3 / KAUN, U.E. and KOEHRING, F.K.A., "Investigations and measures to guarantee the safety of a PWR RPV against brittle fracture", IAEA Meeting Vienna 1984

/ 4 / LABBENS, R., PELLISSIER-TANON, A., HELIOT, J., ASTM STP 590 (1976), 368-384

/ 5 / PETERS, W.H., BLAUEL, J.G., IFKM-Report V 7/79, Freiburg (1979)

/ 6 / ERDOGAN, F., "The study of the effect of cladding on the stress intensity factors in a circumferentially cracked pressure vessel subjected to thermal shock" Report IWM V 13/84, April 1984, and addendum V 13/84*, June 1984

/ 7 / BALL, D.G., CHEVERTON, R.D., DRAKE, J.B., ISKANDER, S.K., Rep. NUREG/CR-3491 ORNL-5934 (1983)

/ 8 / CHELL, G.G., HAIG, J.R. and VITEK, V., Int. J. Fracture 17 (1981) 61-81

/ 9 / HOLLSTEIN, T. and BLAUEL, J.G., "Untersuchungen zum WPS-Effekt", Report IWM V 3/85, März 1985

/ 10 / CRUSE, T.A., BESUNER, P.M., J. of Aircraft 12 (1975), 369-375

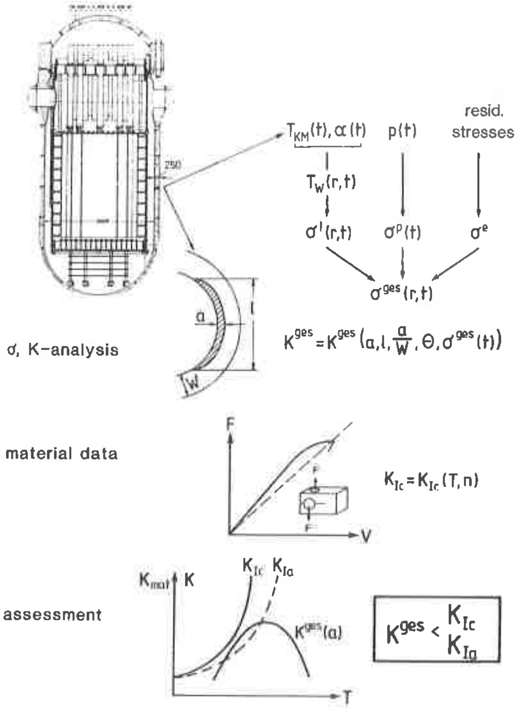

Fig. 1: Fracture mechanics safety analysis of RPV Stade for ECC-conditions

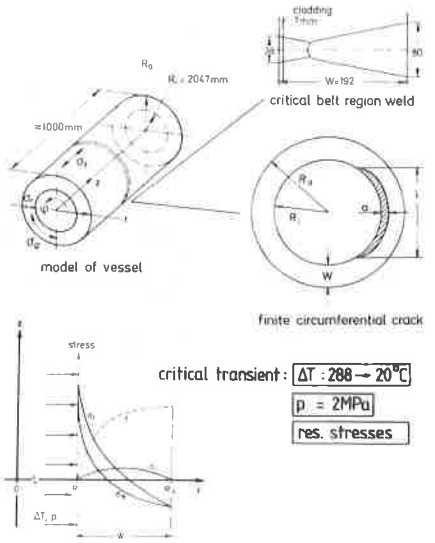

Fig. 2: Geometry and loading conditions

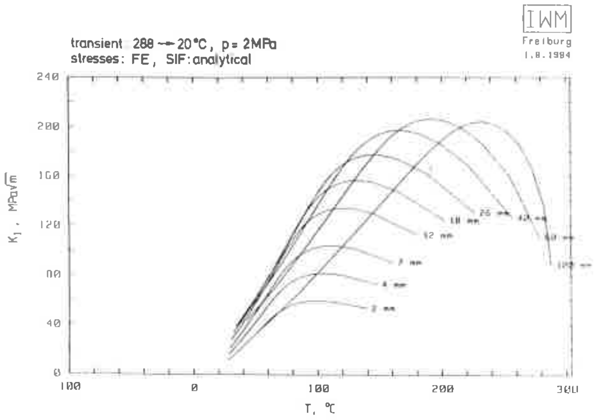

Fig. 3: Resulting SIF`s in the critical transient for circumferential cracks of depth a

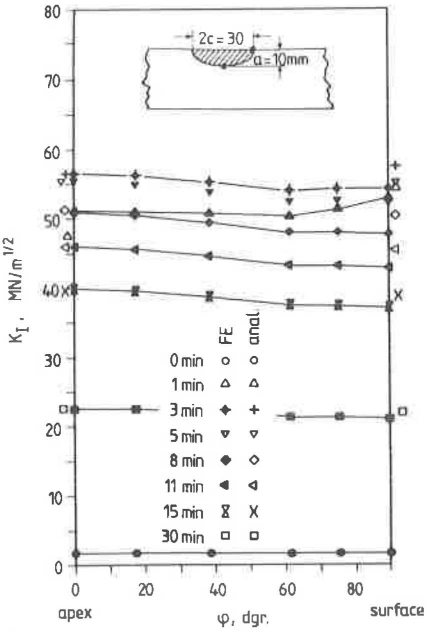

Fig. 4: Stress intensity factors for finite length surface crack, FE calculations and approx. analytical solution

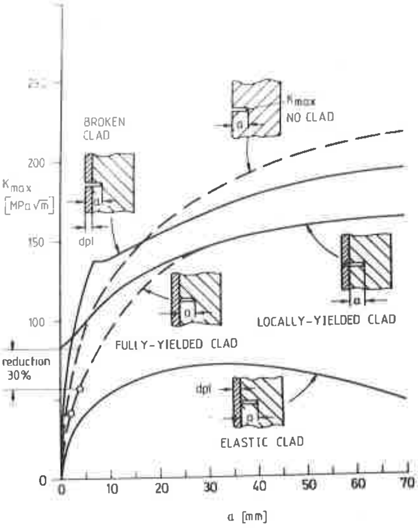

Fig. 5: Influence of 8 mm austenitic cladding on SIF in ferrite

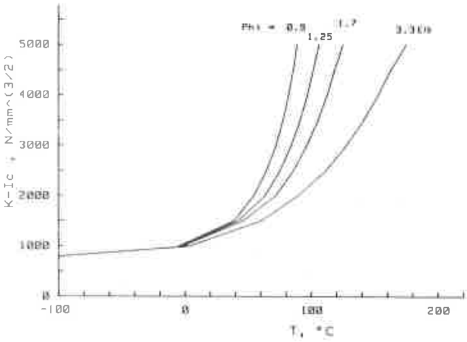

Fig. 6: K_{Ic}-values of high copper weld material as function of neutron fluence and temperature

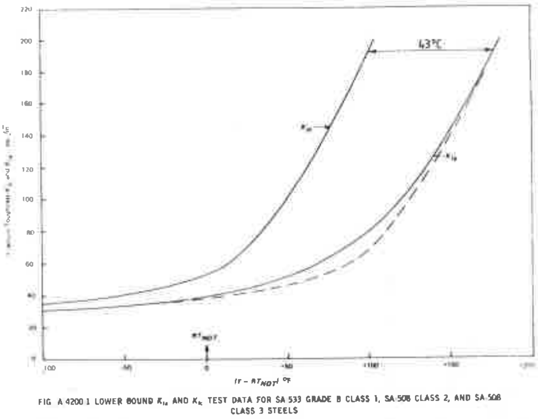

Fig. 7: Derivation of crack arrest toughness K_{Ia} from K_{Ic}-data

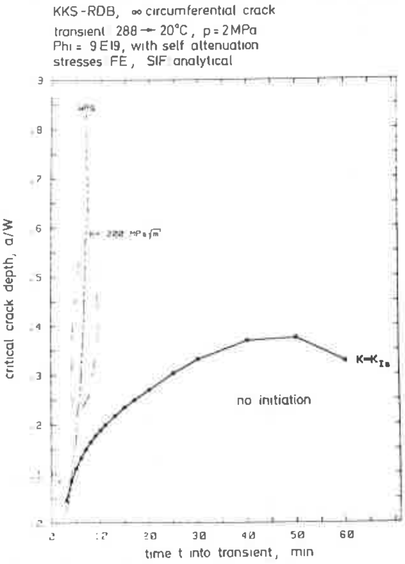

Fig. 8: Critical crack depths for initiation and arrest as function of time in the critical transient

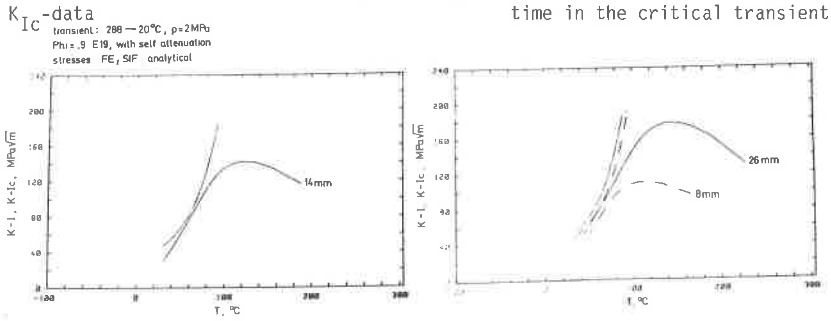

Fig. 9: Alternative description of the assessment situation of Fig. 8

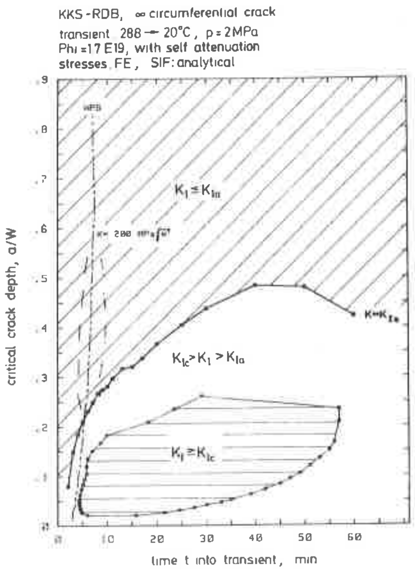

Fig. 10: Assessment situation for EOL-fluence of RPV Stade

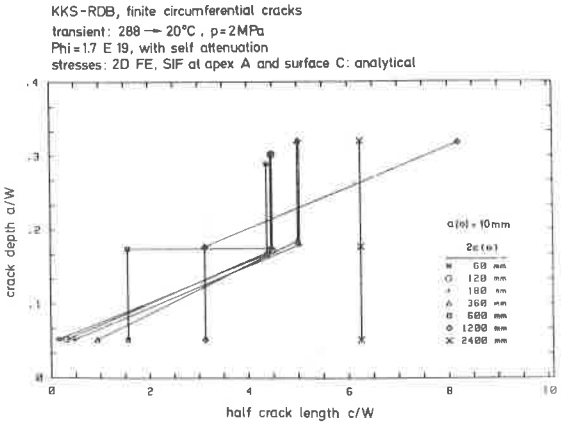

Fig. 11: Crack initiation and arrest analyses for finite length circumferential cracks

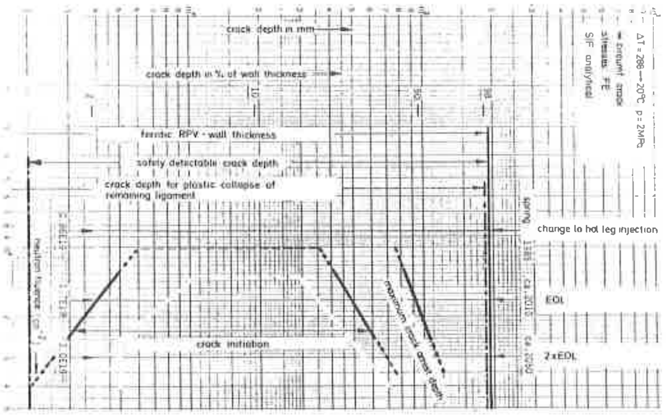

Fig. 12: Summary of safety analysis for RPV Stade